3T MRI of Peripheral Vascular Malformations: Characteristics and Comparison of Two Fat-Saturated sequences: Short Tau Inversion Recovery Versus Three-Dimensional High-Resolution Volume Interpolated Gradient Recalled Echo

3T-MR-Bildgebung peripherer vaskulärer Malformationen – Charakteristiken und Vergleich von 2 fettgesättigten Sequenzen: Short Tau Inversion Recovery versus 3-dimensionale hochauflösende Volume Interpolated Gradient Recalled Echo Sequenz

Authors

Florentine Höhn[1], Simone Hammer[2], Claudia Fellner[2], Florian Zeman[3], Wibke Uller[2], Richard Brill[4], Moritz Guntau[4], Moritz Wildgruber[5], Walter A. Wohlgemuth[4]

Affiliations

1 Clinic and Policlinic of Nuclear Medicine, University Hospital Würzburg, Germany
2 Department of Radiology, University Hospital Regensburg, Germany
3 Centre for Clinical Studies, University Hospital Regensburg, Germany
4 University Clinic and Policlinic of Radiology, Martin Luther University Hospital Halle-Wittenberg, Halle (Saale), Germany
5 Department of Clinical Radiology, University Hospital Münster, Germany

Key words

peripheral vascular malformation, magnetic resonance imaging (MRI), short tau inversion recovery (STIR), volume interpolated breath-hold examination (VIBE), 3.0 Tesla, morphologic characteristics

received 17.11.2019
accepted 26.08.2020
published online 01.10.2020

Bibliography

Fortschr Röntgenstr 2021; 193: 446–458
DOI 10.1055/a-1253-8422
ISSN 1438-9029

Georg Thieme Verlag KG, Rüdigerstraße 14, 70469 Stuttgart, Germany

Correspondence

Florentine Höhn
Clinic and Policlinic for Nuclear Medicine, University Hospital Würzburg, Oberdürrbacherstr. 6, 97080 Würzburg, Germany
Tel.: 0931 201 35422
florentine.hoehn@gmx.de

ZUSAMMENFASSUNG

Ziel Studienziel war es, morphologische und hämodynamische Charakteristiken peripherer vaskulärer Malformationen mittels 3T-Magnetresonanz-Bildgebung prospektiv zu untersuchen und 2 fettgesättigte Sequenzen qualitativ zu vergleichen: die Short Tau Inversion Recovery (STIR) und die 3-dimensionale hochauflösende Volume Interpolated Gradient Recalled Echo (GRE) Sequenz.

Material und Methoden In 9 Monaten wurden 100 Patienten mit V. a. oder mit gesicherter vaskulärer Malformation prospektiv unter Verwendung eines 3T-Scanners mittels einer T2-gewichteten STIR und Turbo-Spin-Echo (TSE), T1-gewichteten TSE und T1-gewichteten, kontrastmittelunterstützten Volume Interpolated Breath-hold Examination (VIBE) untersucht. Zudem wurde eine zeitaufgelöste Magnetresonanzangiografie mit interleaved stochastic trajectories (TWIST-MRA) durchgeführt. Analysiert wurden Signalverhalten, morphologische und hämodynamische Charakteristiken sowie die Bildqualität der 2 fettgesättigten Sequenzen im Vergleich.

Ergebnisse Bei 14 Drop-outs wurden die Daten von 86 Patienten (57 Frauen, 29 Männer; Durchschnittsalter 26,8 Jahre; Altersgruppe 1–56 Jahre) analysiert. Es lagen 22 High-flow- und 64 Low-flow-Malformationen (davon 14 mit lymphatischem Anteil) vor. In 21 der 22 High-flow-Malformationen wurden typische Charakteristiken detektiert (flow-voids, hyperdynamische arteriovenöse Fisteln, dilatierte Haupt-/zuführende Arterien und dilatierte ableitende Venen). Bei den Low-flow-Malformationen kamen in 35 Fällen Phlebolithen, in 47 Flüssigkeits-Flüssigkeitsspiegel und in 23 dilatierte Venen zur Darstellung. Bei den lymphatischen Malformationen zeigte sich eine wandständige Kontrastmittelaufnahme der Zysten. Der Vergleich der fettgesättigten Sequenzen ergab signifikant bessere Ergebnisse der Volume Interpolated GRE in allen untersuchten Kategorien mit Ausnahme der Artefakte, welche in der STIR signifikant geringer ausfielen ($p < 0,05$).

Schlussfolgerung 3T-MR-Bildgebung mit MRA liefert detaillierte morphologische und hämodynamische Informationen zu allen peripheren Malformationstypen. Von den fettgesättigten Sequenzen erwies sich die kontrastmittelgestützte hochauflösende Volume Interpolated GRE bezüglich der Differenzierung morphologischer Charakteristiken der STIR überlegen und diagnostisch aussagekräftig zur Differenzierung lymphatischer Anteile und Gelenkbeteiligungen.

Kernaussagen:

- 3T-MR-Bildgebung mit MRA liefert detaillierte Informationen über alle Malformationstypen.
- Fettgesättigte MR-Sequenzen bilden insbesondere morphologische Charakteristiken, Ausdehnung und Umgebungsinfiltration exakt ab.
- Die Volume Interpolated GRE erwies sich in nahezu allen Kriterien der STIR überlegen.
- Einzige Einschränkung war die höhere Artefaktanfälligkeit der Volume Interpolated GRE.
- Die Volume Interpolated GRE ermöglicht zusätzlich die Differenzierung von lymphatischen Malformationsanteilen sowie Gelenkbeteiligungen.

ABSTRACT

Purpose To assess morphological and hemodynamic characteristics of peripheral vascular malformations on 3 T magnetic resonance imaging (MRI) including qualitative comparison of two fat-saturated sequences: short tau inversion recovery (STIR) and three-dimensional high-resolution volume interpolated gradient recalled echo (GRE).

Materials and Methods During 9 months, 100 patients with suspected or known vascular malformations were prospectively assessed on a 3 T scanner using T2-weighted STIR and turbo spin echo (TSE), T1-weighted TSE, time-resolved contrast-enhanced magnetic resonance angiography (MRA) with interleaved stochastic trajectories (TWIST) and T1-weighted volume interpolated breath-hold examination (VIBE) after contrast enhancement. The analysis included signal behavior and morphologic and hemodynamic characteristics. Additionally, the image quality of the fat-saturated sequences was evaluated by 2 radiologists.

Results 86 patients (14 dropouts; 57 female, 29 male; mean age 26.8 years, age range 1–56) were analyzed. 22 had high-flow and 64 low-flow malformations, including 14 with a lymphatic component. In 21 of 22 patients with high-flow malformations, typical characteristics (flow voids, hyperdynamic arteriovenous fistula, dilated main/feeder-arteries and draining veins) were documented. Patients with low-flow malformations had phleboliths in 35 cases, fluid-fluid levels in 47 and dilated draining veins in 23. Lymphatic malformations showed peripheral contrast enhancement of cyst walls in the volume interpolated GRE. The comparison of fat-saturated sequences showed significantly better results of the volume interpolated GRE in all categories except the presence of artifacts which were significantly reduced in the STIR ($p < 0.05$).

Conclusion 3 T MRI with MRA provides detailed morphological and hemodynamic information of different types of peripheral vascular malformations. Contrast-enhanced high-resolution volume interpolated GRE proved superior to STIR in differentiating morphologic features and to be diagnostic in the differentiation of lymphatic parts and joint involvement.

Key Points:

- 3 T MRI with MRA offers detailed information about vascular malformations.
- Fat-saturated MRI provides especially information about morphological characteristics, extent and tissue involvement.
- Volume interpolated GRE proved superior in almost all categories compared to STIR.
- Volume interpolated GRE showed more artifacts.
- Volume interpolated GRE additionally allows differentiation of lymphatic parts and evaluation of joint involvement.

Citation Format

- Höhn F, Hammer S, Fellner C et al. 3T MRI of Peripheral Vascular Malformations: Characteristics and Comparison of Two Fat-Saturated sequences: Short Tau Inversion Recovery Versus Three-Dimensional High-Resolution Volume Interpolated Gradient Recalled Echo. Fortschr Röntgenstr 2021; 193: 446–458

Introduction

Based on the studies by Mulliken and Glowacki, vascular anomalies can be differentiated into vascular tumors and vascular malformations [1, 2]. Vascular malformations are caused by defective vascular morphogenesis [1, 3], consequently are congenital, and grow proportional to the patient [1, 4, 5], while they are stable from the cellular aspect [1]. Clinically, they can be exacerbated, especially in connection with arteriovenous shunting. Symptoms may range from pain, swelling, impairment of mobility, dysplastic varicose veins, skin changes, recurrent thrombophlebitis, necrosis, erysipelas to lymphorrhea depending on the affected vessel systems and location [6].

The classification of vascular malformations from the International Society for the Study of Vascular Anomalies (ISSVA), which is used worldwide, distinguishes between high-flow malformations, which affect the arterial or arteriovenous system, and low-flow malformations, which affect the venous, capillary, or lymphatic system or combinations thereof [7–9]. Low-flow malformations are generally treated by sclerotherapy [10–13] or laser therapy, while embolization is used in high-flow malformations [11, 14, 15].

In imaging of vascular malformations, ultrasound is limited with respect to its field of view (FOV) and operator dependency. Computed tomographic angiography (CTA) and the invasive digital subtraction angiography (DSA) method provide more detailed

anatomical/hemodynamic information but require ionizing radiation and iodinated contrast medium. Contrast-enhanced magnetic resonance imaging (MRI) – being a less invasive procedure without these risks – is an effective method for assessing affected vessels, as well as the extension of vascular malformations and the involvement of adjacent tissues such as muscle, fat, and bone tissue [11, 16].

Fat-saturated MRI sequences play a key role. Fat-saturated T2-weigthed short tau inversion recovery (STIR) or volume interpolated gradient recalled echo (GRE) imaging highlight vascular malformations within the surrounding fat tissue [17]. T1-weighted delayed venous phases provide the depiction of very-low-flow malformations and the extent of their drainage into the venous system [18–20].

With the progress of technical capabilities, MRI supplemented by magnetic resonance angiography (MRA) has become increasingly important – providing the mandatory morphologic and hemodynamic information for correct diagnosis and treatment planning of vascular malformations [11, 21–23] (such as hyperdynamic arteriovenous fistulas, flow voids, dilated main/feeder arteries or draining veins, phleboliths, and fluid-fluid levels). Dynamic contrast- enhanced MRA with keyhole imaging is known to be the essential sequence to allow detailed evaluation of the architecture and hemodynamic properties of malformations [17]. Parallel imaging as well as interpolation and partial Fourier techniques are usually applied to shorten the acquisition.

The aim of this prospective study was to assess morphological and hemodynamic characteristics of peripheral vascular malformations on 3 T MRI, including a qualitative comparison of the two fat-saturated sequences STIR and volume interpolated GRE.

Materials and Methods

Patients

Institutional review board approval was provided for this prospective study. Informed written consent for MRI examination was obtained from all patients. 100 patients (66 female, 34 male, mean age 27.4 +/– 16.6, age range 0.5–86 years, 32 patients < 18 years) with suspected or known vascular malformation were included on an intention-to-image basis consecutively and prospectively at our multidisciplinary vascular anomalies center during a 9-month period (2011/11–2012/07). The suspected or known diagnosis prior to MRI within the framework of the study was based on anamnestic aspects, clinical findings, color-coded duplex ultrasound, and previously performed computed tomography (CT) or MRI. Patients with known allergic reaction to MR contrast media, certain metal implants, impaired kidney function, or claustrophobia were excluded.

MRI Acquisition

MRI acquisitions were performed on a 3 T magnetic resonance scanner (Magnetom Skyra, Siemens Healthcare, Erlangen, Germany). Depending on the location and extent of the vascular malformation, an appropriate combination of array coils was chosen. The standardized protocol included: T2-weighted STIR and T1-weighted turbo spin echo (TSE) in the coronal plane, T2-weighted STIR in the axial plane, three-dimensional time-resolved contrast-enhanced MRA with interleaved stochastic trajectories (TWIST), T2-weighted TSE in the axial plane and T1-weigthed volume interpolated breath-hold examination (VIBE) in the coronal plane after contrast medium injection. Injection was timed ten seconds after the start of the time-resolved MRA sequence to acquire at least one dataset without contrast medium for subtraction purposes. 0.1 ml/kg body weight of 1.0 M gadobutrol (Gadovist, Bayer Healthcare, Berlin, Germany) followed by 25 ml saline was administered with a flow rate of 2 ml/s by an electronic power injector (Medtron, Saarbrücken, Germany). In cases of a large region of interest, the dose was subdivided – up to three equal portions for three separate MRA datasets – resulting in a total dose of 0.1 ml/ kg body weight. ▶ **Table 1** shows an example of the technical data for the examination of the lower extremities. According to the examined body region, the FOV, pixel size, and slice thickness were adjusted. The TWIST MRA included 21 measurements with a “temporal resolution” of 5.39 seconds, i. e., the time between successive acquisitions of the central k-space parts (Region A); Region B was 20 % indicating that it takes 5 different peripheral acquisitions to fill the entire peripheral k-space. Coronal VIBE images were acquired with a slice thickness of 0.5 and 0.8 mm (according to the examined body region). Axial reconstructions were performed for analysis in this study with a slice thickness of 4 mm. The technical approaches to achieve adequate fat saturation differed. While spectral fat-saturation technique was used for the VIBE, the STIR is characterized by application of a specific inversion pulse.

Evaluation of MRI

Image evaluation was performed visually by two radiologists with 4 and 20 years of experience, blinded to the clinical data and previous imaging in consensus on a PACS workstation. At first, the location, side distribution, distribution pattern, and lesion depth of the vascular malformations were assessed. Signal intensities were gathered in T1 and T2-TSE and T2-STIR sequences and compared to the intensity of muscle tissue. In these three sequences, the presence of phleboliths, fluid-fluid levels, and flow voids were analyzed. Hemodynamic findings like aneurysms, dilated vessels, and direct arteriovenous fistulas were assessed in the TWIST sequence. Information about the contrast medium enhancement pattern of vascular malformations was obtained from the VIBE sequence.

The same reviewers independently evaluated the quality of the fat-saturated sequences STIR and VIBE for each vascular malformation patient – blinded to the clinical data and previous imaging on a PACS workstation. To assess and compare the quality of fat-saturated imaging, nine categories of evaluation criteria were defined similarly to Mostardi et al. [24]. The score of each category ranged from 1–4, with 1 indicating low quality and 4 high quality. The categories 4, 7, and 8 (identification of normal venous structures, vessel sharpness, presence of artifacts, including artifacts due to inconsistency or inhomogeneity of the fat saturation) describe the image quality more generally, while the categories 1, 2, 3, 5, 6, and 9 (identification of the feeding vessel or the filling

▶ **Table 1** Acquisition parameters of all used sequences for the examination of the lower extremities (pelvis, upper leg, knee, lower leg; except feet) of an adult patient with average body measurements.

▶ **Tab. 1** Akquisitionsparameter der verwendeten Sequenzen am Beispiel einer Untersuchung der unteren Extremitäten bds. (Becken, Oberschenkel, Knie, Unterschenkel mit Ausnahme der Füße) eines Erwachsenen mit durchschnittlichen Körpermaßen.

sequence parameter	coronal T2-STIR	coronal T1-TSE	axial T2-STIR	time-resolved 3 D MRA	axial T2-TSE	coronal 3 D GRE VIBE
pixel size in mm × mm	0.73 × 0.73	0.66 × 0.66	0.82 × 0.82	1.08 × 1.08*	0.55 × 0.55	0.88 × 0.88
slice thickness in mm	6.0	6.0	8.0	1.2**	8.0	0.8***
slice gap in mm	0.6	0.6	0.8	–	0.8	–
TR in ms	4490.00	609.00	5180.00	2.62	7750.00	10.50
TE in ms	48.00	11.00	43.00	1.04	91.00	4.59
number of levels	3	3	4	3	4	3
acquisition time in min:s	9:41	6:45	7:20	3 × 2:30	5:08	11:33

* measured pixel size: 1.27 × 1.08 (phase encoding direction × readout direction).
gemessene Pixelkantenlänge: 1,27 × 1,08 (Phasenkodierrichtung × Ausleserichtung).
** measured slice thickness: 1.85 mm.
gemessene Schichtdicke: 1,85 mm.
*** measured slice thickness: 1.00 mm.
gemessene Schichtdicke: 1,00 mm.

nidus, characterization of venous outflow, demonstration of malformation extent, identification of tissue involvement, quality for diagnosis and treatment planning) are specifically related to vascular malformations (▶ **Table 2**).

Statistical Analysis

Analysis was conducted using IBM SPSS Statistics 21.0. The presence of signal features and morphologic and hemodynamic characteristics were summarized by frequency counts and percentages. For the assessment of the quality of fat-saturated imaging, the average scores of both reviewers were determined and the mean criteria score with standard deviation and the median was calculated for each category of STIR and VIBE. To compare the quality of the fat-saturated STIR and VIBE images within the categories, a marginal homogeneity test was used for each reviewer and each category. Values of $p < 0.05$ indicated a significant difference of the quality between the two sequences related to the examined category. To assess the inter-rater agreement, Cohen's kappa was calculated using crosstabs. The inter-rater agreement was evaluated as slight agreement ($k = 0.01–0.20$), fair agreement ($k = 0.21–0.40$), moderate agreement ($k = 0.41–0.60$), substantial agreement ($k = 0.61–0.80$), or almost perfect agreement ($k = 0.81–0.99$).

Results

Patients

14 out of the 100 consecutive patients had to be excluded from the final analysis. Of those, 5 patients were examined twice during the course of the study, 4 patients had another diagnosis (1 case of directly acquired arteriovenous fistula, 1 case of acquired secondary varicosis, 1 case of acquired lymphorrhea due to inflammation, 1 case of infantile hemangioma), 3 patients underwent final MR imaging on a 1.5 T scanner for safety reasons (metallic implants that were not previously mentioned at inclusion, were not removable or were not 3T-compatible), the data of 1 patient was corrupted by artifacts, and the data of another patient was incomplete because of an allergic reaction to the contrast medium. Consequently, data of 86 patients (57 female, 29 male; mean age 26.8, age range 1–56) were analyzed. In 8 cases, the disease was associated with a syndrome: 5 cases of Klippel-Trenaunay syndrome, 1 Bean syndrome, 1 Gorham-Stout syndrome, and 1 Proteus syndrome.

Location, Side Distribution, Distribution Pattern, Lesion Depth

Vascular malformations occurred in the head and neck region (excluding intracranial regions), the thorax, abdomen, and upper and lower extremities. The lower extremities were affected most often (▶ **Table 3**). Only one body region was affected in 73 patients and more than one region was involved in 13 patients (2 body regions in 6 patients, 3 in 4 patients, 4 in 2 patients, 5 in 1 patient). Regarding all 75 patients with involved limbs, the complete limb including the pelvis or shoulder was affected in 36 of these cases. The majority of lesions were unilateral. Bilateral involvement was found in 15 patients. A unifocal distribution pattern was recognized in 49 patients, a multifocal in 20 patients, and a diffuse pattern in 17 patients. Exclusively sub- or epifascial malformations were observed less frequently as compared to combined sub- and epifascial involvement (▶ **Table 3**).

▶ **Table 2** Categories 1–9 with evaluation criteria and aggregate results (mean ± SD) from radiologic evaluation for T2-weighted STIR and VIBE (n = 22 for categories 1–3, n = 86 for categories 4–9). Interrater agreement was listed by Cohen's kappa (Cohen's kappa < 0 no/poor, 0.01–2.0 slight, 0.21–0.40 fair, 0.41–0.60 moderate, 0.61–0.80 substantial, 0.81–1.0 almost perfect interrater agreement) and the significant differences between the results of both sequences by p-value (p-values < 0.05 indicated a statistically significant difference).

▶ **Tab. 2** Kategorien 1–9 mit Evaluationskriterien mit zusammengefassten Ergebnissen (mittlere Bewertungs-Scores +/– Standardabweichung) der radiologischen Evaluation der T2-gewichteten STIR im Vergleich zur VIBE (n = 22 für Kategorie 1–3; n = 86 für Kategorie 4–9). Angabe der Untersucherübereinstimmung mittels Cohens Kappa (Cohens Kappa < 0 keine, 0,01–2,0 sehr schwache, 0,21–0,40 schwache, 0,41–0,60 deutliche, 0,61–0,80 starke; 0,81–1,0 (fast) vollständige Übereinstimmung). Angabe der Signifikanz der Unterschiede zwischen den Sequenzen mittels p-Wert (p-Werte < 0,05 zeigen einen statistisch signifikanten Unterschied an).

categories 1–9 with evaluation criteria after Mostardi et al.	sequence	mean ± std	interrater agreement (Cohen's kappa)	significant difference (p-value)
category 1: identification of feeding vessel(s) 1 = not adequately depicted 2 = marginal 3 = good 4 = excellent	STIR	1.78 ± 0.52	0.80 = substantial	0.006
	VIBE	2.43 ± 0.77	0.64 = substantial	
category 2: identification of filling nidus 1 = not adequately depicted 2 = marginal 3 = good 4 = excellent	STIR	2.18 ± 0.56	0.14 = slight	0.000
	VIBE	3.14 ± 0.67	0.69 = substantial	
category 3: characterization of venous outflow 1 = not adequately depicted 2 = marginal 3 = good 4 = excellent	STIR	2.43 ± 0.57	0.18 = slight	0.001
	VIBE	3.14 ± 0.80	0.59 = moderate	
category 4: identification of normal venous structures 1 = not adequately depicted 2 = marginal 3 = good 4 = excellent	STIR	2.74 ± 0.45	0.50 = moderate	0.000
	VIBE	3.72 ± 0.64	0.61 = substantial	
category 5: demonstration of malformation extent 1 = not adequately depicted 2 = marginal 3 = good 4 = excellent	STIR	2.98 ± 0.68	0.60 = moderate	0.000
	VIBE	3.51 ± 0.78	0.70 = substantial	
category 6: identification of tissue involvement 1 = not adequately depicted 2 = marginal 3 = good 4 = excellent	STIR	3.09 ± 0.52	0.54 = moderate	0.000
	VIBE	3.51 ± 0.72	0.62 = substantial	
category 7: vessel sharpness 1 = poor spatial resolution, little or no definition of structure 2 = slight blurring of vessels, likely to impair diagnosis 3 = good visualization of vessel margins, adequate for diagnosis 4 = excellent visualization of vessel margins	STIR	2.88 ± 0.39	0.40 = fair	0.000
	VIBE	3.86 ± 0.50	0.68 = substantial	

▶ **Table 2** (Continuation)

categories 1–9 with evaluation criteria after Mostardi et al.	sequence	mean ± std	interrater agreement (Cohen's kappa)	significant difference (p-value)
category 8: presence of artifact 1 = severe, nondiagnostic 2 = substantial artifact, mildly/moderately impairs diagnosis 3 = some artifact present, does not impair diagnosis 4 = no artifact	STIR	2.85 ± 0.40	0.88 = almost perfect	0.016
	VIBE	2.70 ± 0.58	0.81 = almost perfect	
category 9: quality for diagnosis and treatment planning 1 = not adequately depicted 2 = marginal 3 = good 4 = excellent	STIR	2.8 ± 0.50	0.38 = fair	0.000
	VIBE	3.51 ± 0.74	0.67 = substantial	

▶ **Table 3** A. Location. B. Side distribution. C. Distribution pattern. D. Lesion depth of the vascular malformations. E. Classification of all peripheral vascular malformations in the study population.

▶ **Tab. 3** A. Lokalisation, B. Seitenverteilung, C. Verteilungsmuster, D. Eindringtiefe, E. Klassifikation aller peripherer vaskulärer Malformationen der Studienpopulation.

general information about peripheral vascular malformations		n = 86
A. location	head and neck	11
	upper extremity	15
	▪ shoulder	6
	▪ upper arm	10
	▪ lower arm	9
	▪ hand	11
	thorax	10
	abdomen	10
	lower extremity	64
	▪ pelvis	38
	▪ upper leg	48
	▪ knee	38
	▪ lower leg	43
	▪ foot	41
B. side distribution	unilateral	71
	bilateral	15
C. distribution pattern	diffuse	17
	focal	69
	▪ unifocal	49
	▪ multifocal	20
D. lesion depth	epifascial	4
	subfascial	16
	epi- and subfascial	66

▶ **Table 3** (Continuation)

general information about peripheral vascular malformations		n = 86
E. classification	high-flow malformations	22
	▪ AVM	18
	▪ AVM and VM	2
	▪ CAVM	2
	low-flow malformations without lymphatic part	50
	▪ VM	37
	▪ CVM	13
	low-flow malformations with lymphatic part	14
	▪ LM	3
	▪ LVM	5
	▪ CVLM	6

AVM: arteriovenous malformation, CAVM: capillary-arteriovenous malformation, CVM: capillary-venous malformation, CVLM: capillary-venous-lymphatic malformation, LM: lymphatic malformation, LVM: lymphatic-venous malformation, VM: venous malformation.
AVM = arteriovenöse Malformation; CAVM = kapillär-arteriovenöse Malformation; CVM = kapillärvenöse Malformation; CVLM = kapillär-venös-lymphatische Malformation; LM = lymphatische Malformation; LVM = lymphatisch-venöse Malformation; VM = venöse Malformation.

Classification

The reference standard to differentiate between high- and low-flow malformations prior to MRI within the framework of the study was based on a combination of anamnestic aspects, clinical findings, color-coded duplex ultrasound and previously performed CT or previously performed MRI if available. The final diagnosis was made in consensus at our Interdisciplinary Vascular

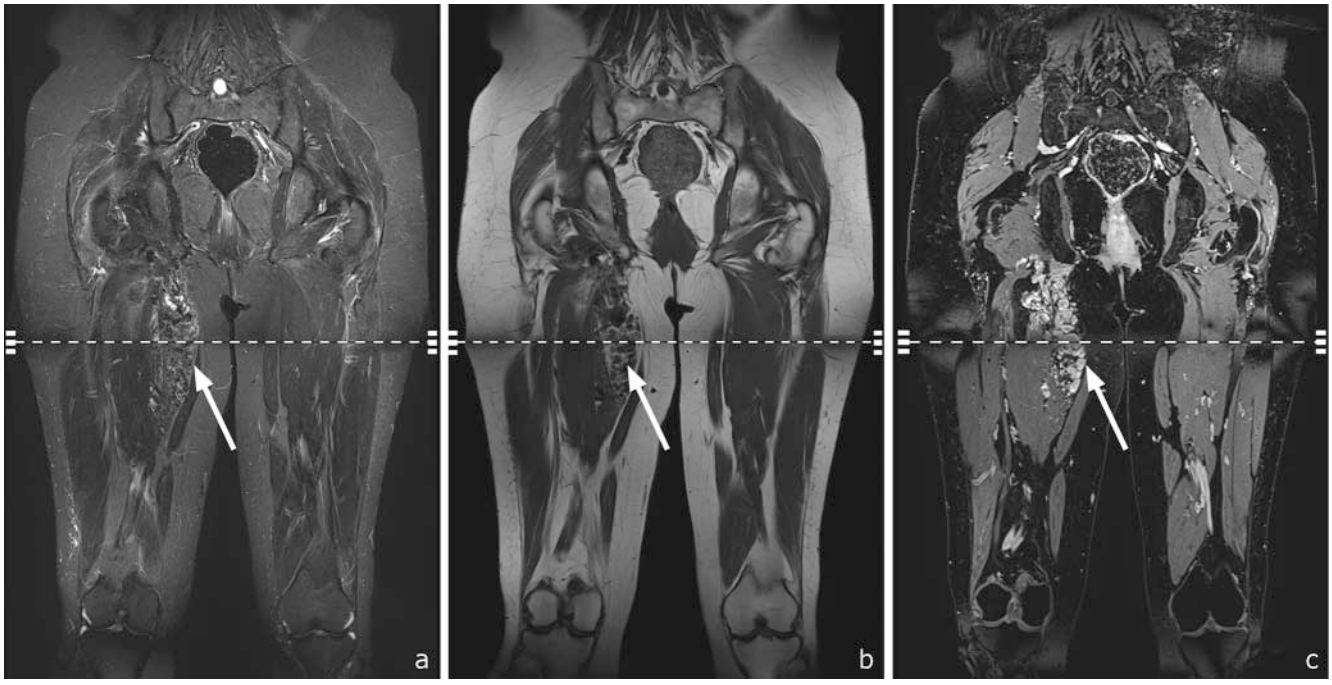

▶ **Fig. 1** 56-year-old female patient with typical arteriovenous malformation of the right leg with flow voids. **a** T2 STIR coronal: hypointense signal. **b** T1 TSE coronal: hypointense signal. **c** 3 D VIBE coronal: homogeneous contrast enhancement.

▶ **Abb. 1** 56-jährige, weibliche Patientin mit typischer arteriovenöser Malformation der rechten unteren Extremität mit flow-voids. **a** T2-STIR coronar: hypointenses Signal. **b** T1-TSE coronar: hypointenses Signal. **c** 3D-VIBE coronar: homogene Kontrastmittelanreicherung.

▶ **Fig. 2** 11-year-old male patient with venous malformation of the right lower leg. **a** T2 STIR coronal: hyperintense signal. **b** T1 TSE coronal: isointense signal. **c** T1 TSE axial: fluid-fluid levels and phleboliths. **d** 3 D VIBE coronal: inhomogeneous contrast enhancement.

▶ **Abb. 2** 11-jähriger, männlicher Patient mit venöser Malformation des rechten Unterschenkels. **a** T2-STIR coronar: hyperintenses Signal. **b** T1-TSE coronar: isointenses Signal. **c** T1-TSE axial: Flüssigkeits-Flüssigkeitsspiegel sowie Phlebolithen. **d** 3D-VIBE coronar: inhomogene Kontrastmittelanreicherung.

Anomalies Center. According to the ISSVA classification, we found 64 low-flow malformations affecting the venous, lymphatic system or both (▶ **Table 3**). 22 patients of the study population had arteriovenous high-flow malformations. Two patients with a simultaneous arteriovenous malformation (AVM) and a venous malformation (VM) were analyzed in the group of AVMs because this was the more dominant diagnosis. Furthermore, a subgroup of AVMs with atypical appearance was found in 7 of the 22 high-flow malformations; they contained less fat tissue, were associated with focal edema, and showed blurred margins and space-occupying aspects similar to a tumor.

STIR, TSE

All vascular malformations showed a hyperintense signal on T2-TSE and STIR images, while they presented with an iso- to hypointense signal on the T1-TSE images. Flow voids as a sign of high blood flow were found in all AVMs and only in one VM without a lymphatic part due to a directly acquired fistula (▶ **Fig. 1**). In contrast to that, phleboliths were present in more than 50 % and fluid-fluid levels in more than 70 % of the low-flow lesions as a sign of low blood flow (▶ **Fig. 2**). AVMs showed neither of them.

Dynamic Contrast-Enhanced MRA with Keyhole Imaging

In all cases with high-flow malformations except one, the afferent feeder arteries as well as all efferent veins were dilated on dynamic contrast-enhanced MRA with keyhole imaging. Furthermore, 4 arterial and 7 venous flow-related aneurysms were found. The AVMs showed very early arterial enhancement, filling of the nidus, and a direct venous outflow, which proved the existence of hyperdynamic arteriovenous fistulas in all cases (▶ **Fig. 3a, b**). Contrary to that, a feeding artery was dilated only in one patient with a low-flow malformation – due to a directly acquired postoperative arteriovenous fistula. Efferent draining communication veins were demonstrated in 36 % of the patients with low-flow malformations. No arterial but 10 venous aneurysms were detected. 62 of the 64 cases exhibited no immediate arterial enhancement pattern, but late contrast pooling in dilated venous channels (▶ **Fig. 3c, d**). In 21 patients with low-flow malformations, a distinct enhancement pattern between the late arterial to early venous phase could be observed. Two directly acquired hyperdynamic arteriovenous fistulas were found due to trauma.

Volume Interpolated GRE

Volume interpolated GRE depicted different enhancement patterns of the contrast medium within the lesions depending on the type of malformation: while AVMs and VMs enhanced homogeneously, lymphatic malformations (LMs) or lymphatic parts of combined venous-lymphatic malformations (VLMs) showed only peripheral enhancement of the cyst walls (▶ **Fig. 4**). Exceptions were three of the "atypical" AVMs, which enhanced inhomogeneously including the surrounding tissue (▶ **Fig. 5**).

▶ **Table 4** summarizes the data of the morphologic and hemodynamic findings in all sequences.

▶ **Fig. 3** 56-year-old female patient with typical arteriovenous malformation of the right upper leg in **a** T2 STIR coronal **b** TWIST with early contrast enhancement of the feeder arteries, the nidus, and the draining veins. 5-year-old female patient with venous malformation of the right upper leg in **c** T2 STIR coronal **d** TWIST with early pooling of the contrast medium within the lesion.

▶ **Abb. 3** 56-jährige, weibliche Patientin mit typischer arteriovenöser Malformation des rechten Oberschenkels in der **a** T2-STIR coronar sowie der **b** TWIST mit nahezu zeitgleicher Kontrastierung der arteriellen Gefäße, der Malformation sowie des venösen Abflusses. 5-jährige, weibliche Patientin mit venöser Malformation des rechten mittleren/distalen Oberschenkels in der **c** T2-STIR coronar sowie der **d** TWIST mit frühem Kontrastmittelpooling in der Gefäßmalformation.

Comparison of Fat-Saturated Imaging: STIR Versus Volume Interpolated GRE

The two fat-saturated sequences, STIR and volume interpolated GRE, of 86 cases were analyzed for their diagnostic value using diagnostic categories independently by two reviewers as stated in ▶ **Table 2** (modified after Mostardi et al.). The value for each category ranged from 1–4 where 1 indicated low image quality and 4 high image quality.

In categories 1–3, average scores of 1.78–2.43 were calculated for STIR, indicating marginal depiction of dynamic information of the vascular malformation, while average scores of 2.43–3.14 were calculated for volume interpolated GRE indicating marginal to good depiction of dynamic information of the vascular malformation. In categories 4–7, average scores of 2.74–3.09 were reached by STIR, indicating good depiction of anatomic information, while average scores of 3.51–3.86 were reached by volume interpolated GRE, indicating excellent depiction of anatomic information. In category 9, STIR was considered good with an average score of 2.80, while volume interpolated GRE was considered excellent with an average score of 3.51.

▶ **Table 4** Summary of morphologic and hemodynamic findings.

▶ **Tab. 4** Überblick über die morphologischen und hämodynamischen Befunde.

	sequence	findings in peripheral vascular malformations		all types of malformations n = 86	high-flow malformations n = 22	low-flow malformations with lymphatic part n = 14	low-flow malformations without lymphatic part n = 50
A	T1-TSE	MRI signal	hypointense	17	13	2	2
			isointense	69	9	12	48
			hyperintense	–	–	–	–
	T2-TSE	MRI signal	hypointense	–	–	–	–
			isointense	–	–	–	–
			hyperintense	86	22	14	50
	T2-STIR	MRI signal	hypointense	–	–	–	–
			isointense	–	–	–	–
			hyperintense	86	22	14	50
B	T2-STIR, T2-TSE, T1-TSE	phleboliths		35	–	8	27
		fluid-fluid levels		47	–	10	37
		flow voids		24	22	–	2
	TWIST	arteriovenous fistulas		51	22	6	23
		▪ hyperdynamic		24	22	–	2
		▪ hypodynamic		27	–	6	21
		aneurysms		21	11	2	8
		▪ arterial		4	4	–	–
		▪ venous		17	7	2	8
	VIBE	enhancement		85	22	14	49
		▪ homogeneous		68	19	–	49
		▪ inhomogeneous		3	3	–	–
		▪ peripheral		3	–	3	–
		▪ combined: homogeneous and peripheral		11	–	11	–

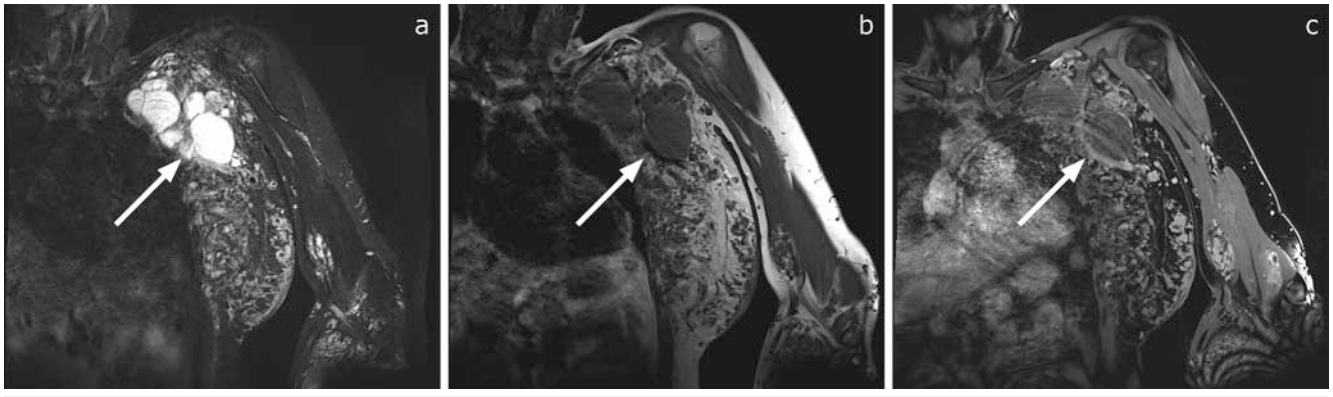

▶ **Fig. 4** 45-year-old female patient with combined venous-lymphatic malformation of the left thorax/mamma and the left arm. **a** T2 STIR coronal: hyperintense signal. **b** T1 TSE coronal: isointense signal. **c** 3 D VIBE coronal: peripheral enhancement of the cyst walls of the lymphatic part.

▶ **Abb. 4** 45-jährige, weibliche Patientin mit kombiniert venös-lymphatischer Malformation der linken Thoraxwand, der linken Mamma sowie der linken oberen Extremität. **a** T2-STIR coronar: hyperintenses Signal. **b** T1-TSE coronar: isointenses Signal. **c** 3D-VIBE coronar: inhomogene, randständige Kontrastmittelanreicherung der zystischen lymphatischen Anteile.

▶ **Fig. 5** 29-year-old female patient with atypical arteriovenous malformation of the right upper leg with blurred margins, less fat tissue, edema and space-occupying aspects similar to a tumor in **a** T2 STIR coronal **b** T1 TSE coronal **c** 3 D VIBE coronal.

▶ **Abb. 5** 29-jährige, weibliche Patientin mit atypischer arteriovenöser Malformation des rechten distalen Oberschenkels mit unscharfer Berandung, vermindertem Fettgewebsanteil, geringem Umgebungsödem, tumorähnlichem raumforderndem Aspekt sowie inhomogener Kontrastmittelanreicherung in der **a** T2-STIR coronar, **b** T1-TSE coronar und **c** 3D-VIBE coronar.

In all mentioned categories, volume interpolated GRE showed significantly better results in comparison to STIR ($p < 0.05$). The only exception was the presence of artifacts in category 8. With an average score of 2.85, STIR proved significantly superior compared to volume interpolated GRE with an average score of 2.70 ($p < 0.05$). All results are summarized in ▶ **Table 2** and examples illustrated in ▶ **Fig. 6**.

The inter-rater agreement was only slight to moderate in categories 1, 2, and 3, whereas in all other categories the inter-rater agreement was fair to almost perfect. In general, the inter-rater agreement of the categories imaged by volume interpolated GRE was the same or superior to STIR. The median of all categories of volume interpolated GRE showed good to excellent results. Within each category the results were spread over all criteria scores. The median of STIR mostly reached marginal to good results with less spread within each category (▶ **Fig. 7**).

Discussion

Technical developments of the last decades have offered an increase in information provided by MRI of vascular malformations. Most prior studies assessed characteristics of vascular malformations in the central nervous system were limited by a small study cohort e. g., [19, 24–27], a retrospective study design, e. g. [25], or lower field strengths, e. g. [25, 27]. The diagnostic quality of the fat-saturated sequences STIR and volume interpolated GRE in relation to vascular malformations has not been compared to date.

Rak et al. [25] and Van Rijswijk et al. [26] assessed MRI of peripheral vascular malformations with lower field strengths of 0.5 T and 1.5 T. Concordantly to Rak et al., the signal of all malformations was hyperintense in the T2-STIR and TSE images, whereas the signal was iso- or hypointense in the T1-TSE images [25]. Furthermore, according to Rak et al. and van Rijswijk et al. [25, 26], we found flow voids in all arteriovenous malformations and in one venous malformation due to a postoperatively acquired direct arteriovenous fistula. As expected, phleboliths and fluid-fluid levels were exclusively seen in venous, lymphatic, or combined lesions. Volume interpolated GRE provided additional information for the differentiation of lymphatic parts by peripheral enhancement of the cyst walls. In principle, the use of a 3 T system adds further diagnostic information within a shorter acquisition time compared to lower field strengths, caused by a higher signal-to-noise ratio [28].

While in the past the differentiation between low-flow and high-flow malformations was mostly performed based on spin-echo MR signal characteristics by assessing the presence of flow voids [25], the use of contrast-enhanced MRI and dynamic contrast-enhanced MRA provided further hemodynamic information for their differentiation [26]. The development of MRA techniques including parallel acquisition with high temporal and spatial resolution, for example the technique of dynamic contrast-enhanced MRA with keyhole imaging, improved the assessment of these hemodynamic characteristics further [23, 27]. Van Rijswijk et al. prospectively assessed if peripheral vascular malformations could

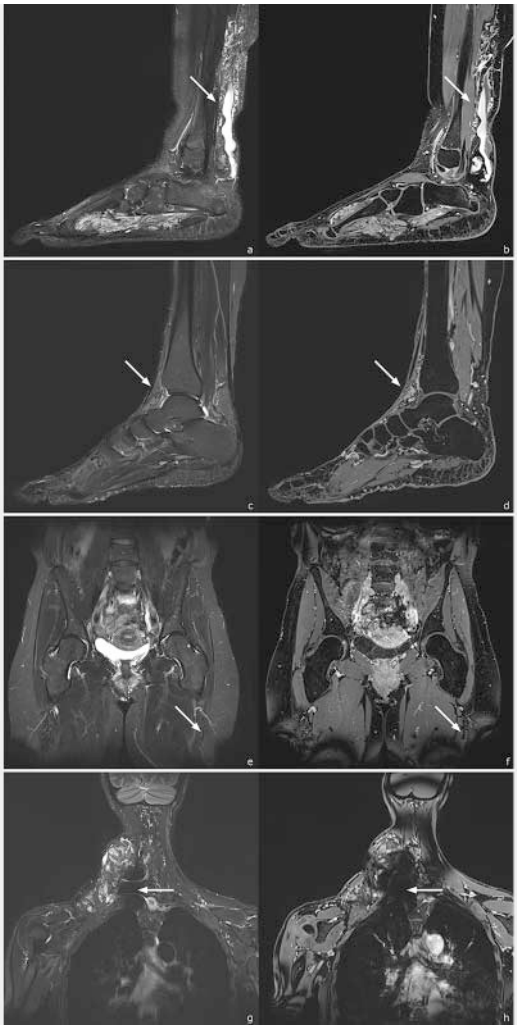

▶ **Fig. 6** Comparison of fat-saturated MRI sequences: STIR on the left and VIBE on the right side of each example. **a, b** Example of superior depiction of the vessels in the VIBE in a 13-year-old female patient with venous malformation of the lower leg and foot in the sagittal plane. **c, d** Example of superior differentiation of the extent of the lesion in the VIBE in a 45-year-old female patient with arteriovenous malformation of the foot in the sagittal plane. **e, f** Example of artifacts due to inhomogeneous fat saturation at the margins of the FOV in 50-year-old female patient with venous malformation of the pelvis in the coronal plane. **g, h** Example of artifacts due to inhomogeneous fat saturation at regions with high differences of susceptibility in a 42-year-old female patient with atypical arteriovenous and venous malformation of the right side of the neck in the coronal plane.

▶ **Abb. 6** Gegenüberstellung der fettgesättigten MR-Sequenzen: STIR auf der linken und VIBE auf der rechten Seite des jeweiligen Beispiels. **a, b** Beispiel überlegener Gefäßdarstellung in der VIBE in 13-jähriger, weiblicher Patientin mit venöser Malformation des Unterschenkels und des Fußes in sagittaler Ebene. **c, d** Beispiel überlegener Differenzierbarkeit der Läsionsausdehnung in der VIBE in 45-jähriger, weiblicher Patientin mit arteriovenöser Malformation des Fußes in sagittaler Ebene. **e, f** Beispiel von Artefakten aufgrund inhomogener Fettsättigung in den Randbereichen des FOV in 50-jähriger, weiblicher Patientin mit venöser Malformation des Beckens in coronarer Ebene. **g, h** Beispiel von Artefakten aufgrund inhomogener Fettsättigung in Regionen mit großen Suszeptibilitätsunterschieden in 42-jähriger, weiblicher Patientin mit atypischer arteriovenöser und venöser Malformation des Halses rechts in coronarer Ebene.

be categorized by dynamic contrast-enhanced MRI. Compared to our results they described early lesion enhancement in malformations with an arterial component as diagnostic criteria besides the presence of flow voids [26]. Ohgiya et al. and Herborn et al. considered the dynamic of contrast enhancement by measuring the contrast rise time that was reasonable to differentiate between high- and low-flow malformations [18, 29]. In our study, a subgroup with differing contrast enhancement was identified within the group of low-flow malformations. Here we hypothesized the presence of hypo-dynamic arteriovenous fistulas. Further scientific study confirmed that [30].

In our study cohort some multifocal/diffuse and bilateral lesions were found, the majority of lesions were combined sub- and epifascial. Rak et al. already described the multifocal nature of VMs and the risk of symptomatic exacerbation after incomplete therapy [25]. These aspects need to be considered for therapy planning (by scanning contralateral sides or adjacent body parts) to capture the whole lesion. Volume interpolated GRE and STIR are preferably used to describe the morphologic characteristics and to demonstrate the extent of the malformations as well as the involvement of surrounding and involved tissues. The complete three-dimensional imaging by volume interpolated GRE allows exact evaluation of joint involvement (▶ **Fig. 8**). Numerous observed changes in the surrounding tissue, such as edema, fat/muscle, and bone hyper- and hypoplasia, differing lengths of extremities or arthritis make further studies indispensable.

By comparing the quality of fat-saturated imaging of the malformations in this study, we could show that contrast-enhanced volume interpolated GRE proved superior in almost all diagnostic categories as compared to STIR. Despite the superior diagnostic image quality of volume interpolated GRE, its vulnerability to artifacts was higher. GRE sequences are in general more vulnerable to artifacts than TSE sequences. Especially, volume interpolated GRE datasets acquired with a large FOV or in regions with inherently high differences in magnetic susceptibility (such as the neck) showed less homogeneous fat saturation in comparison to the STIR datasets, due to the used spectral fat-saturation technique of water excitation. This could be the reason for the wider spread observed over all criteria scores within each category of the volume interpolated GRE sequence. Nevertheless, the inter-rater agreement of the categories for volume interpolated GRE was the same or superior to that of STIR, indicating a lower interpreter dependency of volume interpolated GRE. Homogeneous and artifact-reduced fat saturation is of clinical importance to evaluate the complete extent of the lesion in therapy planning as well as in follow-up to exclude incomplete or inadequate therapy. Further studies about the sensitivity to various artifacts could help to refine MR protocols.

In our study, the analysis of the categories describing the dynamic information of the vascular malformations was limited because those were initially designed to assess vascular malformations with dynamic contrast-enhanced MRA, whereas we compared morphologic sequences. Consequently, the lowest scores were reached in categories 1, 2, and 3. In these categories, the inter-rater agreement was only slight to moderate, whereas in all other categories it was fair to almost perfect. Aside from the mentioned limitation of the design of the categories, both morphologic fat-saturated sequences are limited concerning the dynamic

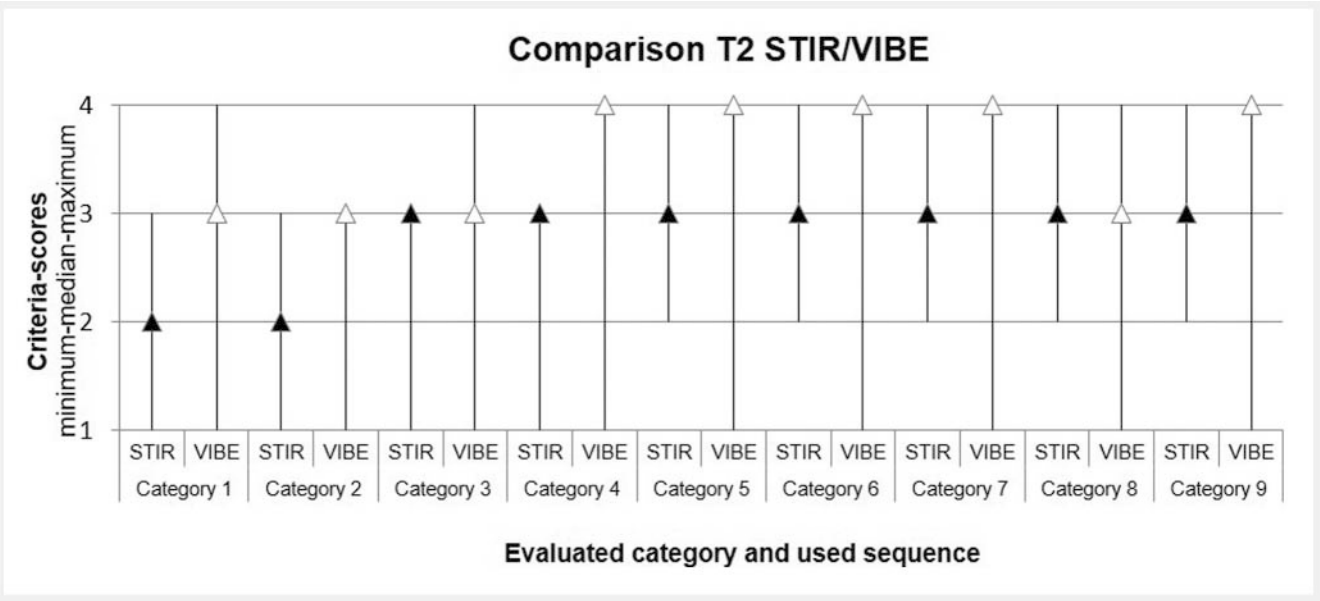

▶ **Fig. 7** Achieved criteria scores (minimum, median, maximum) of the evaluated categories using T2-weighted STIR and 3 D VIBE in comparison based on Mostardi et al.

▶ **Abb. 7** Streubreite der erreichten Bewertungs-Scores (Minimum, Maximum und Median auf Höhe des Pfeils) der T2-gewichteten STIR im Vergleich zur T1-gewichteten 3D-VIBE in den jeweiligen Kategorien nach Mostardi et al.

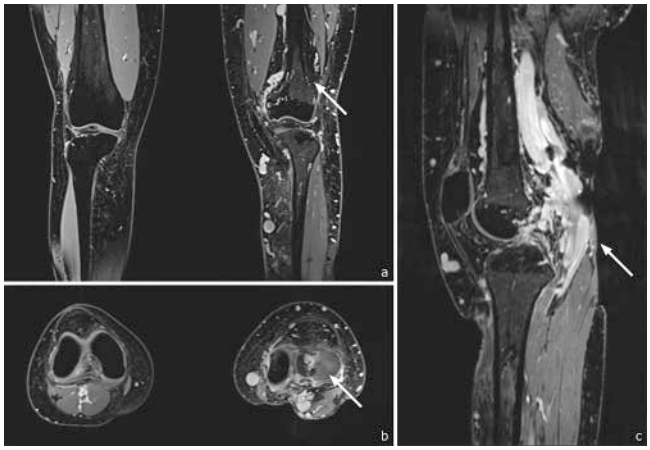

▶ **Fig. 8** 26-year-old female patient with typical arteriovenous malformation of the left leg with involvement of the knee joint in the 3 D VIBE sequence in **a** coronal **b** axial and **c** sagittal plane, reconstructed from the coronal 3 D data set.

▶ **Abb. 8** 26-jährige Patientin mit typischer arteriovenöser Malformation der unteren Extremität mit Kniebeteiligung in der 3D-VIBE **a** coronar, **b** axial sowie **c** sagittal, rekonstruiert aus dem coronaren 3D-Datensatz.

flow information as compared to dynamic contrast- enhanced MRA with keyhole imaging. The study may also be limited by the fact that some of the patients had already undergone previous therapy, as this might affect the MRI-based presentation of the vascular malformation. In general, the cohort of the study was very heterogeneous, which might affect the results as well.

Conclusion

3 T MRI supplemented by time-resolved MRA provided detailed and additional information about morphological and hemodynamic characteristics of peripheral vascular malformations, allowing for a clear diagnosis according to the ISSVA classification. Three-dimensional volume interpolated GRE proved to be diagnostic in the differentiation of lymphatic parts and evaluation of joint involvement.

In the comparison of the quality of fat-saturated imaging of peripheral vascular malformations, contrast-enhanced volume interpolated GRE proved superior in all categories except artifact-proneness compared to STIR with respect to differentiating morphologic features of vascular malformations.

CLINICAL RELEVANCE OF THE STUDY

- Due to different treatment strategies, correct classification of peripheral vascular malformations is indispensable.
- Large/multifocal/bilateral lesions require optimized MRI protocols to offer detailed hemodynamic and morphologic information in an acceptable acquisition time.
- The diagnostic quality of MR sequences relating to peripheral vascular malformations needs to be evaluated to optimize MRI protocols.

Conflict of Interest

The authors declare that they have no conflict of interest.

References

[1] Mulliken JB, Glowacki J. Hemangiomas and vascular malformations in infants and children: A classification based on endothelial characteristics. Plast Reconstr Surg 1982; 69: 412–422. doi:10.1097/00006534-198203000-00002

[2] Enjolras O, Mulliken JB. Vascular tumors and vascular malformations (new issues). Adv Dermatol 1997; 13: 375–423

[3] Enjolras O, Wassef M, Chapot R. Color atlas of vascular tumors and vascular malformations. Cambridge University Press. 2007; 1st ed. 1–12. doi:https://doi.org/10.1017/CBO9780511722073

[4] Enjolras O. Classification and management of the various superficial vascular anomalies: hemangiomas and vascular malformations. J Dermatol 1997; 24: 701–710. doi:10.1111/j.1346-8138.1997.tb02522.x

[5] Garzon MC, Huang JT, Enjolras O et al. Vascular malformations Part I. J Am Acad Dermatol 2007; 56: 353–370. doi:10.1016/j.jaad.2006.05.069

[6] Wohlgemuth WA, Wölfle K, Schuster T et al. Angeborene Gefäßmalformationen: Klassifikation, Symptome, Diagnostik und Prognose. Zentralbl Chir 2012; 137: 440–445. doi:10.1055/s-0030-1262546

[7] Behr GG, Johnson C. Vascular anomalies: Hemangiomas and beyond – Part 1, fast-flow lesions. Am J Roentgenol 2013; 200: 414–422. doi:10.2214/Am J Roentgenol.11.7852

[8] Behr GG, Johnson CM. Vascular anomalies: Hemangiomas and beyond – Part 2, slow-flow lesions. Am J Roentgenol 2013; 200: 423–436. doi:10.2214/ajr.11.7853

[9] Wassef M, Blei F, Adams D et al. Vascular anomalies classification: Recommendations from the International Society for the Study of Vascular Anomalies. Pediatrics 2015; 136: e203–e214. doi:10.1542/peds.2014-3673

[10] Lee BB, Kim DI, Huh S et al. New Experiences with absolute ethanol sclerotherapy in the management of a complex form of congenital venous malformation. J Vasc Surg 2001; 33: 764–772. doi:10.1067/mva.2001.112209

[11] Müller-Wille R, Wildgruber M, Sadick M et al. Vascular anomalies (Part II): Interventional therapy of peripheral vascular malformations. Fortschr Röntgenstr 2018; (EFirst) doi:10.1055/s-0044-101266

[12] Ali S, Mitchell SE. Outcomes of venous malformation sclerotherapy: A review of study methodology and long-term results. Semin Intervent Radiol 2017; 34: 288–293. doi:10.1055/s-0037-1604300

[13] Qiu Y, Chen H, Lin X et al. Outcomes and complications of sclerotherapy for venous malformations. Vasc Endovascular Surg 2013; 47: 454–461. doi:10.1177/1538574413492390

[14] Do YS, Park KB, Cho SK. How do we treat arteriovenous malformations (tips and tricks)? Tech Vasc Interv Radiol 2007; 10: 291–298. doi:10.1053/j.tvir.2008.03.008

[15] Yakes WF, Rossi P, Odink H. How do I do it? Arteriovenous malformation management. Cardiovasc Intervent Radiol 1996; 19: 65–71. doi:10.1007/bf02563895

[16] Dubois J, Alison M. Vascular anomalies: what a radiologist needs to know. Pediatr Radiol 2010; 40: 895. doi:10.1007/s00247-010-1621-y

[17] Majewska NK, Stajgis P, Wykrętowicz M et al. Peripheral vascular malformations – modern imaging. Pol J Radiol 2018; 83: 253–259. doi:10.5114/pjr.2018.75724

[18] Herborn CU, Goyen M, Lauenstein TC et al. Comprehensive time-resolved MRI of peripheral vascular malformations. Am J Roentgenol 2003; 181: 729–735. doi:10.2214/ajr.181.3.1810729

[19] Kociemba A, Karmelita-Katulska K, Stajgis M et al. Distinguishing high-flow from low-flow vascular malformations using maximum intensity projection images in dynamic magnetic resonance angiography – comparison to other MR-based techniques. Acta Radiol 2016; 57: 565–571. doi:10.1177/0284185115615005

[20] Donnelly LF, Adams DM, Bisset GS 3rd. Vascular malformations and hemangiomas: a practical approach in a multidisciplinary clinic. Am J Roentgenol 2000; 174: 597–608. doi:10.2214/ajr.174.3.1740597

[21] Hyodoh H, Hori M, Akiba H et al. Peripheral vascular malformations: Imaging, treatment approaches, and therapeutic issues. Radiographics 2005; 25: 159–172. doi:10.1148/rg.25si055509

[22] Moukaddam H, Pollak J, Haims AH. MRI characteristics and classification of peripheral vascular malformations and tumors. Skeletal Radiol 2009; 38: 535–547. doi:10.1007/s00256-008-0609-2

[23] Kim JS, Chandler A, Borzykowski R et al. Maximizing time-resolved MRA for differentiation of hemangiomas, vascular malformations and vascularized tumors. Pediatr Radiol 2012; 42: 775–784. doi:10.1007/s00247-012-2359-5

[24] Mostardi PM, Young PM, McKusick MA et al. High temporal and spatial resolution imaging of peripheral vascular malformations. J Magn Reson Imaging 2012; 36: 933–942. doi:10.1002/jmri.23714

[25] Rak KM, Yakes WF, Ray RL et al. MR imaging of symptomatic peripheral vascular malformations. Am J Roentgenol 1992; 159: 107–112. doi:10.2214/ajr.159.1.1609682

[26] Van Rijswijk CSP, Van der Linden E, Van der Woude HJ et al. Value of dynamic contrast-enhanced MR imaging in diagnosing and classifying peripheral vascular malformations. Am J Roentgenol 2002; 178: 1181–1187. doi:10.2214/ajr.178.5.1781181

[27] Kramer U, Ernemann U, Mangold S et al. Diagnostic value of high spatial and temporal resolution time-resolved MR angiography in the workup of peripheral high-flow vascular malformations at 1.5 Tesla. Int J Cardiovasc Imaging 2012; 28: 823–834. doi:10.1007/s10554-011-9887-1

[28] Heidemann RM. Magnetresonanztomografie bei hohen Feldstärken: Ist stärker besser? Max-Planck-Institut für Kognitions- und Neurowissenschaften Leipzig, Jahrbuch 2007/2008. Im Internet (Stand: 23.10.2019): https://www.cbs.mpg.de/3177/research_report_384338?c=7551

[29] Ohgiya Y, Hashimoto T, Gokan T et al. Dynamic MRI for distinguishing high-flow from low-flow peripheral vascular malformations. Am J Roentgenol 2005; 185: 1131–1137. doi:10.2214/ajr.04.1508

[30] Hammer S, Uller W, Manger F et al. Time-resolved magnetic resonance angiography (MRA) at 3.0 Tesla for evaluation of hemodynamic characteristics of vascular malformations: description of distinct subgroups. Eur Radiol 2017; 27: 296–305. doi:10.1007/s00330-016-4270-1